Contrib Mineral Petrol (1994) 118:1–12

John N. Christensen · Jane Selverstone · John L. Rosenfeld · Donald J. DePaolo

Correlation by Rb-Sr geochronology of garnet growth histories from different structural levels within the Tauern Window, Eastern Alps

Received: 25 October 1993 / Accepted: 21 April 1994

Abstract In order to evaluate rates of tectonometamorphic processes, growth rates of garnets from metamorphic rocks of the Tauern Window, Eastern Alps were measured using Rb-Sr isotopes. The garnet growth rates were determined from Rb-Sr isotopic zonation of single garnet crystals and the Rb-Sr isotopic compositions of their associated rock matrices. Garnets were analyzed from the Upper Schieferhülle (USH) and Lower Schieferhülle (LSH) within the Tauern Window. Two garnets from the USH grew at rates of $0.67^{+0.19}_{-0.13}$ mm/million years and $0.88^{+0.34}_{-0.19}$ mm/million years, respectively, indicating an average growth duration of 5.4 ± 1.7 million years. The duration of growth coupled with the amount of rotation recorded by inclusion trails in the USH garnets yields an average shear-strain rate during garnet growth of $2.7^{+1.2}_{-0.7} \times 10^{-14}$ s^{-1}. Garnet growth in the sample from the USH occurred between 35.4 ± 0.6 and 30 ± 0.8 Ma. The garnet from the LSH grew at a rate of 0.23 ± 0.015 mm/million years, between 62 ± 1.5 Ma and 30.2 ± 1.5 Ma. Contemporaneous cessation of garnet growth in both units at ~30 Ma is in accord with previous dating of the thermal peak of metamorphism in the Tauern Window. Correlation with previously published pressure-temperature paths for garnets from the USH and LSH yields approximate rates of burial, exhumation and heating during garnet growth. Assuming that these $P - T$ paths are applicable to the garnets in this study, the contemporaneous exhumation rates recorded by garnet in the USH and LSH were approximately 4^{+3}_{-2} mm/year and 2 ± 1 mm/year, respectively.

J. N. Christensen[1](✉) · J. L. Rosenfeld
Department of Earth and Space Sciences, University of California, Los Angeles Los Angeles, CA 90024, USA

D. J. DePaolo · J. N. Christensen
Center for Isotope Geochemistry, Department of Geology and Geophysics, University of California, Berkeley, and Earth Sciences Division, Lawrence Berkeley Laboratory, Berkeley, CA 94720, USA

J. Selverstone
Department of Geological Sciences, University of Colorado, Boulder, CO 80309-0250, USA

[1]*Present address*
Department of Geological Sciences, University of Michigan, 1006 C. C. Little Bldg, Ann Arbor, MI 48109, USA

Editorial responsibility: J. Patchett

Introduction

The connection between the pressure-temperature history of a metamorphic rock and the tectonic history of a mountain belt has been investigated during the past decade through the development of petrologic techniques for the reconstruction of metamorphic pressure-temperature-time (*P-T-t*) paths. The interpretation of *P-T-t* paths has been aided and guided by modeling of the thermal behavior of crust during tectonic events. A critical constraint, though, for understanding such paths and their implications for the tectonics of collisional belts is the calibration in time of the metamorphic path (Cliff 1985; Zeitler 1989; Blanckenburg et al. 1989; Mezger et al. 1990). Recently, much progress has been made toward the measurement of rates and timing of prograde processes in metamorphic rocks (e.g., Mezger et al. 1989; Christensen et al. 1988, 1989; Vance and O'Nions 1990, 1992; Burton and O'Nions 1991). These efforts have focused mainly on garnet, which can grow and persist over a large range in temperature and pressure. In addition, for geological cooling rates and common grain sizes, garnet has relatively high closure temperatures for the Pb (Mezger et al. 1989), Sr (Coghlan 1990) and perhaps Nd (Mezger et al. 1992) isotopic systems such that it is likely to record growth ages at all but the highest metamorphic grades.

Christensen et al. (1989) demonstrated for garnets of Acadian age from SE Vermont, USA, that Sr isotopic zonation recorded within garnet can be used to

measure the growth rates of individual garnets. The two main assumptions of this method are: (1) the matrix from which the garnet grew was essentially homogeneous with respect to $^{87}Sr/^{86}Sr$; (2) the change in $^{87}Sr/^{86}Sr$ recorded by garnet during its growth is due to *in situ* decay of ^{87}Rb in the matrix. In this paper we present data for both the timing and duration of growth of garnets from samples of the Upper Schieferhülle (USH) and the Lower Schieferhülle (LSH), which represent two contrasting structural levels within the Tauern Window, Eastern Alps. Dating and measuring the duration of garnet growth in samples from these two units provide constraints on the tectonometamorphic history of the Tauern Window. Garnets from the Upper Schieferhülle record extensional shear deformation (Selverstone 1985, 1988), which with the duration of garnet growth provides a measure of the shear-strain rate during garnet growth. Estimates of the pressure-temperature history (*P-T* path) of garnet growth in the USH and LSH were made by Selverstone and Spear (1985), Selverstone et al. (1984), Selverstone and Munoz (1987) and Selverstone (unpublished data) for the same general localities studied here. Assuming that these *P-T* paths are applicable to the garnets studied here, they can be correlated and calibrated in time. The Rb-Sr isotopic measurement of the duration of garnet growth thus permits calculation of rates of burial, exhumation and heating during garnet growth.

Geologic setting

The Tauern Window exposes the Penninic nappes from beneath the Austro-Alpine nappes that were emplaced during the Alpine Orogeny. The Penninic series within the window consists of three structural units (Mortcani 1974; Janoschek and Matura 1980; Selverstone 1985) (Fig. 1). The lowest is the Zentralgneis, which consists mainly of polymetamorphic rocks of Hercynian age. Structurally above the Zentralgneis is the Lower Schieferhülle, which is the Paleozoic and parautochthonous Permo-Mesozoic cover to the Zentralgneis. The highest unit is the Upper Schieferhülle, an allochthonous Mesozoic series of greenstones, calc-mica schists and pelitic schists. The boundaries of the Tauern Window are defined by thrust and normal fault contacts with the overlying Austro-Alpine nappes.

Metamorphism of the Penninic units in the Eastern Alps reflects subduction of the Neo-Tethys ocean basin beneath the Adriatic plate in Late Cretaceous time, followed by continent-continent collision between Europe and Adria in the Tertiary. The resultant overthickening of the crust and/or changes in relative motion between Europe and Adria led to crustal extension from at least Early Oligocene through Miocene times. This tectonic history is recorded by *P-T-t* paths in the USH and LSH that show early burial at low temperatures, subsequent heating to temperatures of 475–550° C, and significant decompression under nearly isothermal conditions (Selverstone 1988, and references therein).

Description of samples

Determination of garnet growth durations using the Rb-Sr isotopic techniques of Christensen et al. (1989) requires samples containing large garnets ($\geq$ 5 mm diameter) with few inclusions in a micaceous matrix. Ideally we should have used the samples characterized in previous *P-T* studies (e.g. Selverstone et al. 1984; Selverstone and Spear 1985; Selverstone and Munoz 1987) for isotopic analysis, but none of those samples met all of the necessary criteria. The samples used in this study are thus from different outcrops, but within the same general vicinity (see below) as the samples for which *P-T* data are available. The absence of any known structural discordances between the sample localities described by Selverstone and those of the present study suggests that the existing *P-T* path data can be correlated in a general way with the samples used in this study.

Garnets were analyzed from two schist samples, HF-9a and PJ-8h from the western Tauern Window. Sample HF-9a is from the Upper Schieferhülle (USH) and was collected within 500 m of USH samples HF-6 and HF-27 described by Selverstone and Spear (1985). Sample PJ-8h is from the Lower Schieferhülle (LSH) (Fig. 1) at locality (1) described by Selverstone and Munoz (1987); this locality is 3 km SW of the FH-1 samples discussed by Selverstone et al. (1984).

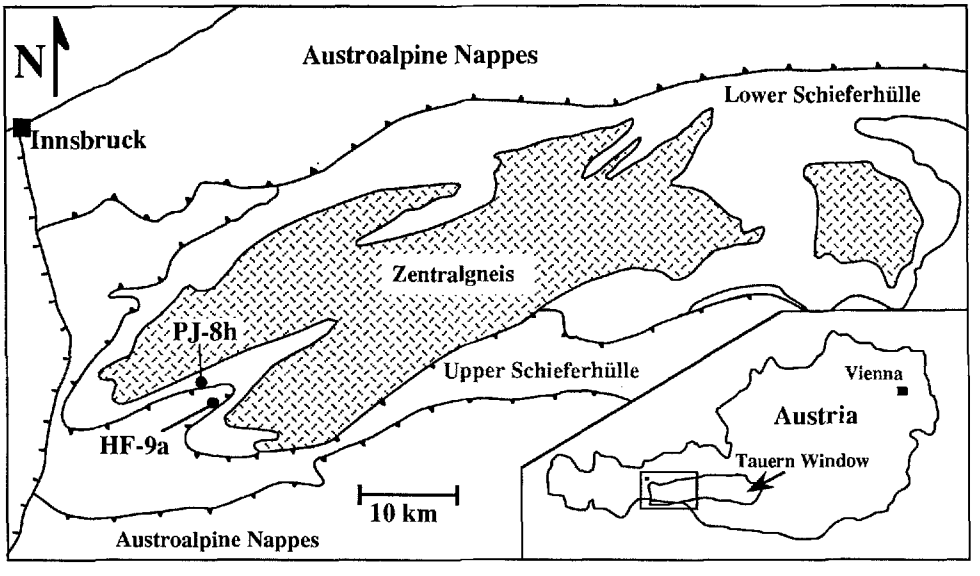

Fig. 1 Geologic sketch map of the western Tauern Window, Italy and Austria. Locations of Upper Schieferhülle sample HF-9a and Lower Schieferhülle sample PJ-8h are indicated by *black dots*. After Selverstone et al. 1991

The matrix of HF-9a (USH) consists of quartz, white mica (paragonite and phengite), ilmenite, biotite and some chlorite. Feldspar is absent from this sample. Garnet porphyroblasts contain inclusions of ilmenite and quartz, as well as rare chloritoid, biotite and tourmaline. Chloritoid is not present in the matrix. Garnet growth was synkinematic as indicated by snowball textures; similar features have been recognized throughout the USH in this area (Selverstone and Spear 1985).

The matrix of PJ-8h consists of quartz, white mica, biotite, ilmenite and plagioclase (oligoclase) with trace amounts of epidote, carbonate and apatite. Chlorite appears to be secondary after biotite, although some may be primary. Most biotite crystals show no alteration to chlorite, but rare examples exist of biotite surrounded by orthoclase that in turn is surrounded by chlorite.

Garnet porphyroblasts in PJ-8h have inclusions of quartz, ilmenite and rare carbonate and rare epidote with allanite cores. The foliation defined by variations in the distribution of matrix quartz passes essentially undisturbed into garnet, indicating that garnet growth was postkinematic. The garnets of the Lower Schieferhülle do not in general exhibit snowball or rotational features (Selverstone 1985). Cracks are present in the garnets, some of which are filled with chlorite.

Sample preparation and analytical techniques

Two garnets were selected from the Upper Schieferhülle sample (garnets HF-9a garnet A and HF-9a garnet B) and one garnet from PJ-8h, a Lower Schieferhülle sample, for Sr isotopic analysis. In addition, from HF-9a a 1.1 g matrix sample (Mx 1) from around garnet A and a 4.6 g matrix sample (Mx 2) from around garnet B were analyzed. For sample PJ-8h, a 48 g whole rock sample was analyzed as well as a 0.4 g matrix sample taken from around the analyzed garnet.

To cut the garnets, a low speed diamond saw with a 0.15 mm thick blade was used. From each of the garnets a disk was cut that passed through the garnet center. Next, a rod was cut out along the diameter of the disk, perpendicular to a pair of opposing faces of the crystal. This rod was then sectioned into a series of segments. These segments form core to rim traverses for each garnet. The positions of the sample segments for each garnet are shown schematically in Fig. 2. For garnet A from HF-9a a core and two different rim segments were analyzed, whereas for garnet B, core, intermediate and rim segments were analyzed. From the PJ-8h garnet, "core", intermediate and rim segments plus an "edge" sample representing the last 500 μm of garnet growth were analyzed. The PJ-8h "core" segment is not from the exact center of the garnet, based on an electron microprobe traverse of the garnet.

Before crushing the garnet segments, they were cleaned in acetone, weighed and their dimensions measured. The crushed garnet segments were sieved and the 60–100 and 40–60 mesh size fractions, checked for inclusions, and then were leached in dilute HF and HCl. The segments were dissolved using ~2 ml HF/mg sample and 1 ml $HClO_4$/mg sample in closed teflon vials, heated to ~100 °C overnight. The 100 mg aliquots of the matrix powders were dissolved in a similar fashion. Further details of the analytical procedure can be found in Christensen (1992).

For each garnet segment Sr and Rb concentrations were determined by isotope dilution using a mixed spike; separate ^{84}Sr and ^{87}Rb spikes were used for the matrix samples. For each garnet segment a 1 mg aliquote was made to which a mixed $^{87}Rb - ^{84}Sr$ spike was added. This was loaded without separation directly on a Re filament for the determination of Sr and Rb concentrations. The Sr from the dissolved garnet and matrix samples was separated using a cation exchange column as described by Christensen (1992). For a 100 mg sample the total chemistry blank for Sr was $\leq$ 100 pg and was negligible in all cases. The Sr isotopic analyses were carried out on a VG Sector 54 multi-collector mass spectrometer using the dynamic mode. For all samples at least two separate Sr isotopic analyses were run and a weighted average value of $^{87}Sr/^{86}Sr$ was calculated for each sample. In general analyses of matrix and segments of the same garnet were made in the same barrel run (16 samples plus 4 standards per barrel). Segments run at later times were analyzed along with duplicate analyses of previously run segments. If necessary, the result for the previously run segment was corrected to the value obtained in the earlier barrel run. This correction was then applied to the analysis of the new segment.

Electron microprobe rim to rim traverses of each garnet were made for major element composition. Mounts for these analyses were made from unused portions of the same garnets analyzed for their isotopic compositions; consequently the microprobe traverses do not pass through the center of the crystals. The results of the electron microprobe traverses for HF-9a garnet B and the PJ-8h garnet are presented in Fig. 3.

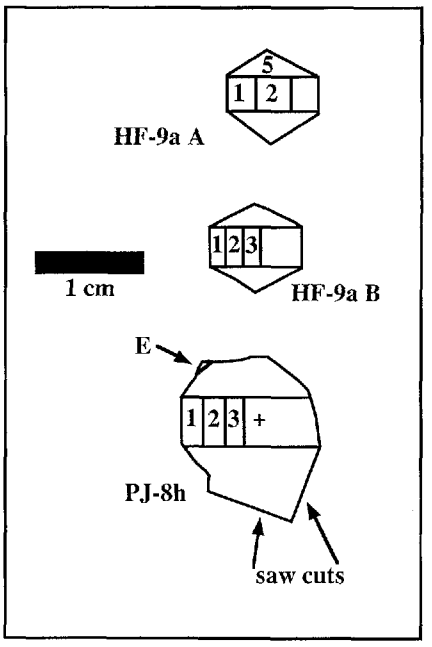

Fig. 2 Schematic representation of garnets A and B from HF-9a and the PJ-8h garnet showing the locations of analyzed garnet segments

Analytical results

Sr concentration zonation of garnet

The results of the garnet isotopic traverses indicate that the garnets are zoned in Sr concentration (Table), although the nature of the zoning is different for each sample. The two garnets from HF-9a (USH) are zoned in a similar manner, with higher Sr concentration in the core than in the rim (Fig. 4). In contrast, the garnet from PJ-8h (LSH) has higher overall Sr concentration and is zoned in the opposite sense, from about 39 ppm in the "core" to 60 ppm in the outer 500 μm of the garnet (Fig. 4). For the PJ-8h garnet, Sr concentration shows a monotonic linear increase from "core" to rim.

The most crucial question to consider here is whether or not the measured Sr concentrations represent Sr held in the garnet structure or a mixture of

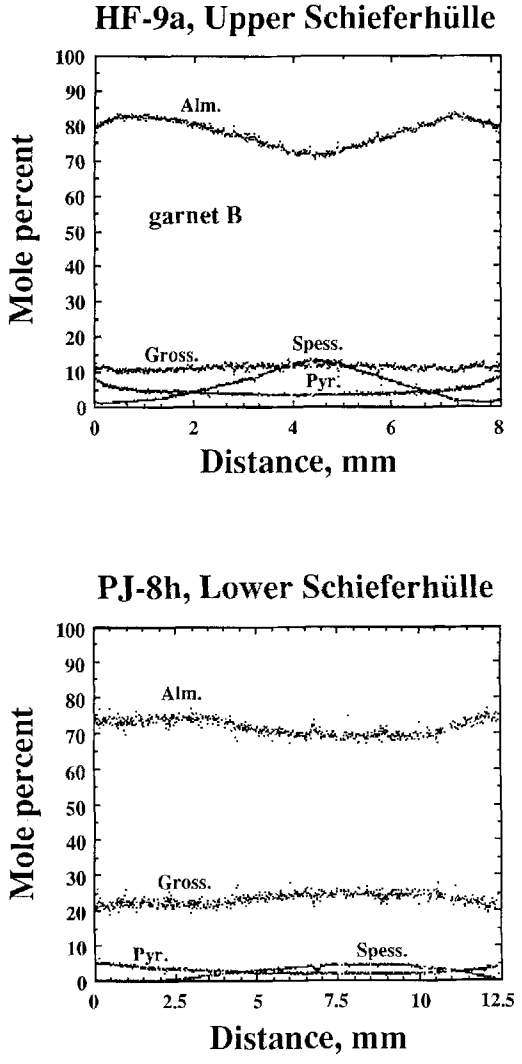

Fig. 3 Rim to rim electron microprobe traverses of garnet B from HF-9a and of the PJ-8h garnet

garnet and inclusion Sr. If most of the Sr comes from mineral inclusions, then the age indicated by a matrix/garnet pair may reflect the age of the inclusions rather than of the garnet.

In the case of the garnets from HF-9a, no inclusions were identified that could significantly contribute to the Sr concentration of an individual garnet segment. In addition, the Sr zoning pattern is consistent between the two analyzed garnets. Therefore we conclude that the bulk of the Sr in the HF-9a garnets is in the garnet itself rather than in inclusions. The garnets of PJ-8h, as noted above, contain rare inclusions of epidote that contain upward of 7000 ppm of Sr (from electron microprobe analysis). Therefore, a single grain of epidote 100 μm on a side would contain ~ 25 ng of Sr. Because the epidote inclusions are rare and heterogeneously distributed, the observed Sr zoning is most likely due to real variation in the concentration of Sr in garnet. Also, the rims of the garnets were observed to be inclusion free. Though it is not proven, we consider it safe to assume that the bulk of the Sr in the analyzed Tauern Window garnets is contained in garnet and not in inclusions.

Partitioning of a trace element between garnet and the bulk matrix depends in part on the affinity of garnet for the element. The variation of Sr concentration in garnet among the samples and the observed Sr zonation within garnet may be tied to variations in the major element composition of the garnets. Probably Sr^{2+} occupies the eight-coordinated site in garnet, where the major cations Mg, Fe, Mn and Ca reside. The affinity of garnet for Sr depends on the size of the eight-coordinated site, which in turn depends on the occupancy of the octahedral site. Figure 5 shows the region of stable garnet structures for compatible combinations of the ionic radii of the octahedral ion and the eight-coordinated ion (Novak and Gibbs 1971). Because Sr^{2+} has an ionic radius of 1.26 Å (Shannon 1976), the size of the eight-coordinated site is too small when the octahedral site is occupied by Al^{3+} but large enough when it is occupied by Fe^{3+}, Ti^{4+}, Ti^{3+}, V^{3+} or by Cr^{3+} (Fig. 5). Occupancy of the octahedral site by Ti^{4+} would require the substitution $Y^{2+} + Ti^{4+} = 2Al^{3+}$, where Y^{2+} may be Fe^{2+} or Mg^{2+}, etc. (Huggins et al. 1977), also increasing the size of the eight-coordinated site. Therefore the partitioning of Sr into the garnet should increase as the Fe^{3+}, Ti, V^{3+} or Cr^{3+} concentration of the garnet increases. This effect may be important even if the concentration of Fe^{3+} is only a few tenths of a percent. From the above, it appears that increasing the Ca content of garnet does not necessarily increase Sr partitioning.

The partitioning of Sr into garnet is about 10 times greater for the PJ-8h garnet than the HF-9a garnet. As might be expected from the Sr concentration difference, the Ca content of the HF-9a garnet is less than that of the PJ-8h garnet, though by only a factor of about two (Fig. 3). The Ca content of the PJ-8h garnet decreases by about 5% from core to rim, the opposite sense shown by the Sr concentration. The HF-9a garnet is essentially unzoned in Ca content. Therefore, although there is some relationship between Ca content and Sr partitioning, the Sr concentration zoning does not correlate directly with Ca zoning.

Unfortunately, the TiO_2 and Cr_2O_3 concentrations are barely detectable by electron microprobe analysis (detection limit about 4000 ppm). Zoning in these elements, if present, is thus not detected. Sample PJ-8h has high formula Si which is an indication of unaccounted Fe^{3+} (Schumacher 1991), but no significant andradite zoning at a level of several tenths of a percent appeared from a Fe^{3+} correction (method of Schumacher 1991). In a garnet from a different LSH sample, Hickmott et al. (1987) found zoning in trace elements including Cr and Ti, but Ti concentration decreased from core to rim whereas Cr was constant. At present we cannot conclude that zoning in Ti, Fe^{3+} and/or Cr^{3+}

Table 1 Sr and Rb isotopic data for matrix and garnets from samples HF-9a (Upper Schieferhülle) and PJ-8h (Lower Schieferhülle). The analytical uncertainty in garnet $^{87}Rb/^{86}Sr$ is about 1%, while error in matrix and whole rock $^{87}Rb/^{86}Sr$ is about 0.5%. Reported average $^{87}Sr/^{86}Sr$ values are weighted according to the uncertainties of the individual measurements. $^{87}Sr/^{86}Sr$ of segments and matrix for an individual garnet were conducted in a single analytical run of the mass spectrometer, except in the case of ga E from PJ-8h. $^{87}Sr/^{86}Sr$ analysis of PJ-8h segment E (edge) was conducted at a later time than the rest of the segments. Also analyzed at the same time as segment E were replicate analyses of segment PJ-8h gal, average $^{87}Sr/^{86}Sr$ indicated by (\$). The average $^{87}Sr/^{86}Sr$ of segment E was corrected to (*) using the difference between the original average value of segment ga 1 and the average of its replicate analyses (\$)

Sample no.	Position	Rb, ppm	Sr, ppm	$^{87}Rb/^{86}Sr$	$^{87}Sr/^{86}Sr \pm 2\sigma$	$(^{87}Sr/^{86}Sr)_{average}$
HF-9a, ga 1	Rim	0.23	3.3	0.209	0.723971 ± 7	0.723971 ± 5
					0.723970 ± 7	
HF-9a, ga 5	Rim, 2nd	0.45	3.8	0.341	0.724022 ± 7	0.724009 ± 5
					0.724002 ± 9	
					0.723981 ± 13	
HF-9a, ga 2	Core	0.96	5.5	0.501	0.723768 ± 9	0.723777 ± 5
					0.723771 ± 9	
					0.723787 ± 9	
					0.723780 ± 9	
HF-9a, Mx 1	Matrix for ga	329.0	167.9	5.681	0.726329 ± 9	0.726350 ± 5
					0.726366 ± 9	
					0.726356 ± 10	
HF-9a, gb 1	Rim	0.16	3.6	0.126	0.723918 ± 7	0.723918 ± 7
					Failed	
HF-9a, gb 2	Intermediate	0.22	4.4	0.144	0.723790 ± 9	0.723797 ± 6
					0.723803 ± 9	
HF-9a, gb 3	Core	0.19	4.5	0.1185	0.723620 ± 9	0.723624 ± 8
					0.723635 ± 14	
HF-9a, Mx 2	Matrix for gb	307.5	174.8	5.103	0.726147 ± 9	0.726151 ± 6
					0.726154 ± 7	
PJ-8h, ga E	Edge	0.72	59.8	0.035	0.710642 ± 9	0.710634 ± 5
					0.710628 ± 7	0.710665 ± 5*
					0.710662 ± 11	
					0.710625 ± 7	
PJ-8h, ga 1	Rim	0.34	57	0.0175	0.710620 ± 9	0.710620 ± 5
					0.710615 ± 7	
					0.710629 ± 9	
					0.710586 ± 7	0.710589 ± 5$^{\$}$
					0.710583 ± 17	
					0.710592 ± 7	
PJ-8h, ga 2	intermediate	0.11	47.5	0.00698	0.710479 ± 9	0.710464 ± 5
					0.710467 ± 9	
					0.710447 ± 9	
PJ-8h, ga 3	Core	0.12	38.7	0.0091	0.710305 ± 9	0.710282 ± 5
					0.710297 ± 9	
					0.710260 ± 7	
PJ-8h, Mx	Matrix for ga	79.9	205.2	1.127	0.711161 ± 10	0.711168 ± 6
					0.711171 ± 7	
PJ-8h, WR	Whole rock	57.1	158.5	1.044	0.711162 ± 7	0.711160 ± 5
					0.711168 ± 10	
					0.711151 ± 9	

correlates with Sr concentration zoning, but we strongly suspect that it does.

Sr isotopic zonation of garnet

The results of the Sr and Rb isotopic analyses of the garnet traverses and associated matrix samples of HF-9a and PJ-8h are presented in Table 1. Both garnets from sample HF-9a of the USH are zoned with respect to $^{87}Sr/^{86}Sr$ (Fig. 6a, b). Garnet A shows an increase between the core and rim in $^{87}Sr/^{86}Sr$ (Fig. 6a). The two rim samples from garnet A have very similar Sr isotopic evolution lines and nearly identical intercepts with the evolution line of matrix Mx 1. The consistency of these two samples, which were taken from positions separated by 90° along the garnet rim, indicates that the matrix was homogeneous with respect to $^{87}Sr/^{86}Sr$ at the scale of the garnet diameter (8 mm) at the time of garnet growth. Garnet B also shows an increase from core to rim in $^{87}Sr/^{86}Sr$ (Fig. 6b). Taken together, the intersections of the isotopic evolution lines of the garnet A and garnet B segments and the Mx 1 and Mx 2 samples demonstrate that the isotopic zonation is consistent between the two garnets (Fig. 7). This is further evidence that during the period of garnet growth, the matrix was homogeneous with respect to $^{87}Sr/^{86}Sr$, at least at the scale (~2 cm) of separation of the analyzed garnets.

The garnet from the LSH, sample PJ-8h, is also isotopically zoned, with monotonically increasing $^{87}Sr/^{86}Sr$ from "core" to rim (Fig. 8). The garnet

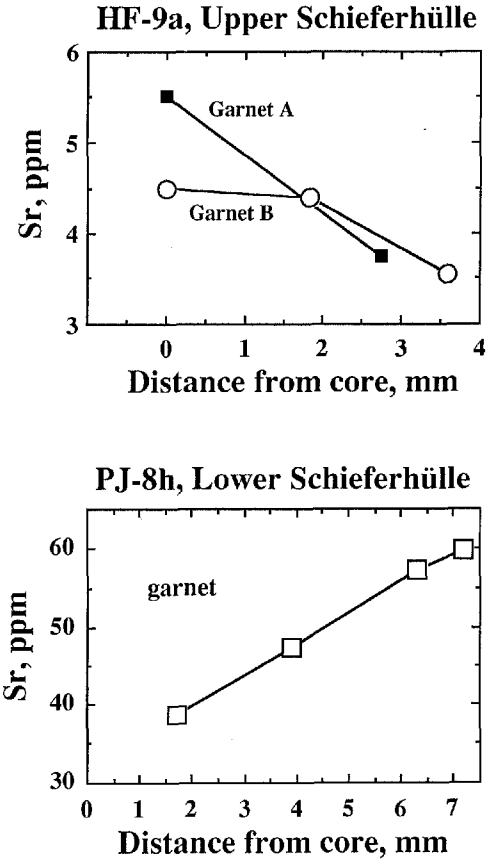

Fig. 4 Distance from garnet core (mm) versus Sr concentration (ppm) for the analyzed segments from (*top*) HF-9a garnets A and B and (*bottom*) for the analyzed segments of the PJ-8h garnet. Sr concentration in both HF-9a garnets decreases from core to rim. In the Ph-8h garnet, Sr concentration shows a very regular increase from core to rim

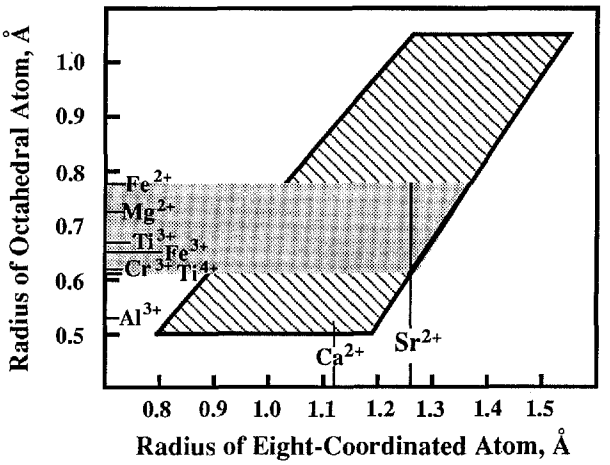

Fig. 5 Region of compatible combinations of the ionic radii of the eight-coordinated atom and the ionic radii of the octahedral atom after Novak and Gibbs (1971, Fig. 9). Shown are the ionic radii of Al^{3+}, Fe^{3+}, Cr^{3+}, V^{3+}, $Ti^{4+,3+}$, Mg^{2+}, Fe^{2+} (octahedral site occupancy) and the ionic radii of Sr^{2+} and Ca^{2+} (Shannon 1976). For Al^{3+} octahedral occupancy the eight fold site is too small for Sr^{2+}. Ionic radii of Fe^{3+}, Cr^{3+}, V^{3+}, Ti^{3+}, Ti^{4+}, Mg^{2+} or Fe^{2+} define a band (*grey*) which provides for the ionic radius of Sr^{2+}. Substitution of Ti^{4+} into the octahedral site would require the coupled substitution of a doubly valent cation such Mg^{2+} or Fe^{2+} into the octahedral site (Huggins et al. 1977)

segments have low $^{87}Rb/^{86}Sr$, from 0.007 to 0.035, so their evolution lines have very shallow slope. This shallow slope results in a correction of only 5 to 20×10^{-6} in $^{87}Sr/^{86}Sr$ for an age of 50 Ma; thus, even an error of 10% in the $^{87}Rb/^{86}Sr$ of the segments would have a negligible effect on the age-corrected $^{87}Sr/^{86}Sr$ values.

Diffusive movement of Sr within the garnets and diffusive exchange between garnet and the surrounding matrix should be negligible. Using a diffusivity of 10^{-21} cm^2/s (based on diffusion parameters of Coghlan 1990) for a temperature of 570° C, over a period of 10 million years the characteristic diffusive distance for Sr in garnet would be ~ 10 μm. Alternatively, using the same diffusion parameters (Coghlan 1990), the closure temperature for Sr diffusion in a 0.5 mm diameter garnet at a cooling rate of 1° C/million years would be ~ 620°C. This is well above the maximum temperatures reached by the LSH (520–550° C) and USH (475° C) in the sampled area (Selverstone et al. 1984; Selverstone and Spear 1985; Selverstone and Munoz 1987).

Garnet growth histories

The Rb-Sr isotopic data in the Table can be used to calculate two-point isochrons between successive garnet segments and the appropriate matrix sample. The USH matrix samples have $^{87}Rb/^{86}Sr$ of 5.68 and 5.10, which implies a resolution of 130 ka, whereas the LSH matrix has an $^{87}Rb/^{86}Sr$ of 1.13 and a resolution of 625 ka. The uncertainties, though, in the ages presented below were calculated based on the uncertainties in the Rb-Sr isotopic compositions of both the garnet segments and the matrix samples.

The HF-9a garnet A core and matrix (Mx 1) give an age of 35.0 ± 0.6 Ma and the two rims give ages of 30.6 ± 0.5 Ma and 30.9 ± 0.5 Ma. The segments of HF-9a garnet B with its matrix (Mx 2) yield ages of 35.7 ± 0.6 Ma (core), 33.4 ± 0.5 Ma (intermediate), 31.6 ± 0.5 Ma (rim). The analyzed segments of the LSH garnet give ages, from the "core" outward, of 55.8 ± 1.3 Ma, 44.2 ± 1.1 Ma, 34.8 ± 1.0 Ma, and 32.2 ± 1.3 Ma.

Plotting the ages of the segments versus their position within each of the garnets produces garnet growth history curves. The core and rim ages of HF-9a garnet A (Fig. 9a) indicate that the garnet grew at an average rate of $0.67^{+0.19}_{-0.13}$ mm/million years, assuming a constant dr/dt. The ages of the HF-9a garnet B segments (Fig. 9b) correlate linearly with their positions within the garnet, indicating growth at a constant rate of

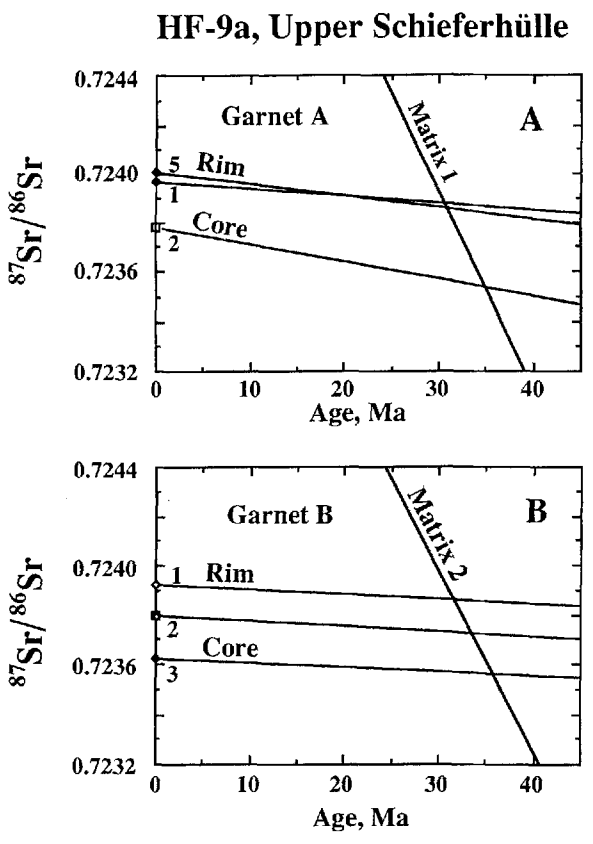

Fig. 6A, B Sr evolution diagrams for garnet segments and matrix samples from sample HF-9a, Upper Schieferhülle. The slopes of the evolution lines are proportional to $^{87}Rb/^{86}Sr$. The intersections between the evolution lines of garnet segment and matrix sample indicates the age of segment. **A** Garnet A and its associated matrix sample The evolution lines of the two different rim segments of garnet A have very similar intersections with the matrix sample. This indicates that the matrix was homogeneous with respect to $^{87}Sr/^{86}Sr$ at the scale of the garnet diameter. **B** Garnet B and its associated matrix sample. The core, intermediate and rim segments indicate an increasing matrix $^{87}Sr/^{86}Sr$ during garnet growth

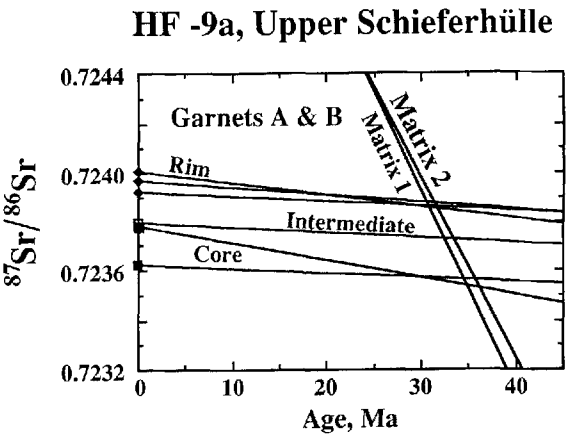

Fig. 7 Sr evolution diagram showing together the evolution lines of both garnets A and B segments and matrix samples. Both garnets record a similar increase in matrix $^{87}Sr/^{86}Sr$ indicating that the matrix was homogeneous with respect to $^{87}Sr/^{86}Sr$ at the scale of separation, ~ 2 cm, of garnets A and B

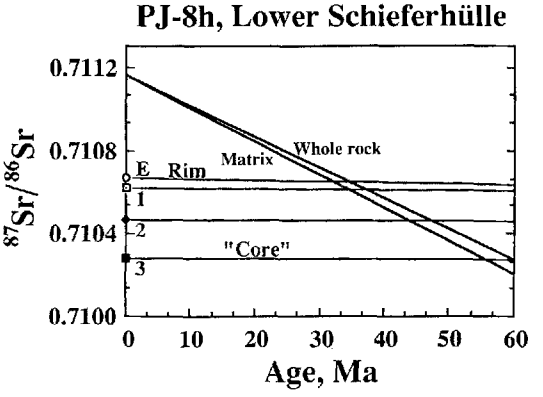

Fig. 8 Sr evolution diagram for the PJ-8h garnet segments, the associated matrix and a whole rock sample. The garnet shows a very regular increase in $^{87}Sr/^{86}Sr$ from core to rim

$0.88^{+0.34}_{-0.19}$ mm/million years. Extrapolation of the garnet A growth rate to its true rim indicates a total growth time of 6.0 ± 1.0 million years and an age of 29 ± 1 Ma for the cessation of garnet growth. A similar extrapolation for garnet B yields a total growth time of 4.8 ± 1.2 million years and cessation of garnet growth at 30.8 ± 1.2 Ma. The growth rates of the USH garnets are just within error of the growth rates (average $= 1.4^{+0.9}_{-0.5}$ mm/million years) measured by Christensen et al. (1989) of Acadian age garnets from Vermont and the rate obtained ($1.9^{+2.9}_{-0.7}$ mm/million years) by Vance and O'Nions (1992) for a garnet from the Central Alps. The growth rate of a Taconic age garnet from Newfoundland has been estimated to be between 1.3 and 19.0 mm/million years (Vance and O'Nions 1990).

On a plot of age versus distance within the garnet the ages of the LSH segments closely approximate a straight line, indicating that the LSH garnet also grew at a nearly constant dr/dt (Fig. 10). The slope of the best-fit line gives an average growth rate of 0.23 ± 0.015 mm/million years, which is slower than the growth rate of garnet from the Central Alps (Vance and O'Nions 1992). Extrapolation of this rate to the true rim of the garnet indicates an age of 30.2 ± 1.5 Ma for the cessation of garnet growth. The true core (based on the major element zoning) of the LSH garnet began growth at 62 ± 1.5 Ma, assuming the linear extrapolation is valid. The LSH garnet from PJ-8h therefore grew over an interval of ~32 ± 2 million years. That both the USH garnet B and the LSH garnet appear to have grown at an essentially constant rate has important implications for the kinetics of garnet growth which will be explored in a separate publication (J. N. Christensen, D. J. DePaolo and J. L. Rosenfeld in preparation).

The differences between the ages of the garnet segments are better known than their individual ages. The uncertainty in the age differences of the segments depends on the uncertainties in the $^{87}Sr/^{86}Sr$ of the

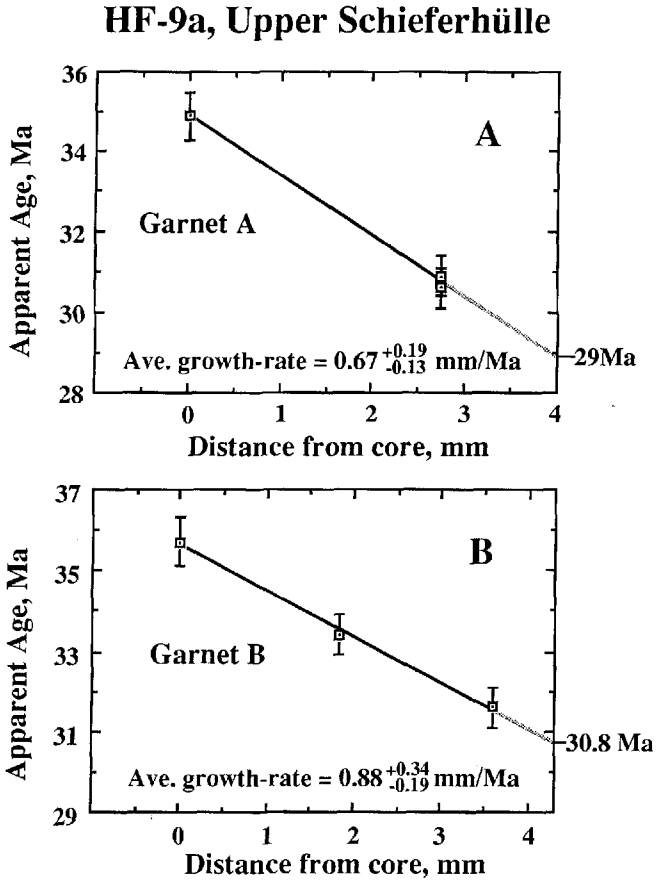

Fig. 9A, B Plots of the position of the center of a garnet segment relative to the core versus the segment age. Also plotted are the extrapolated ages of the edges of the garnets. **A** Garnet A from HF-9a, Upper Schieferhülle. **B** Garnet B from HF-9a. The uncertainties in segment ages are based on the uncertainties in the Rb-Sr isotopic analysis of the garnet segments and matrix samples

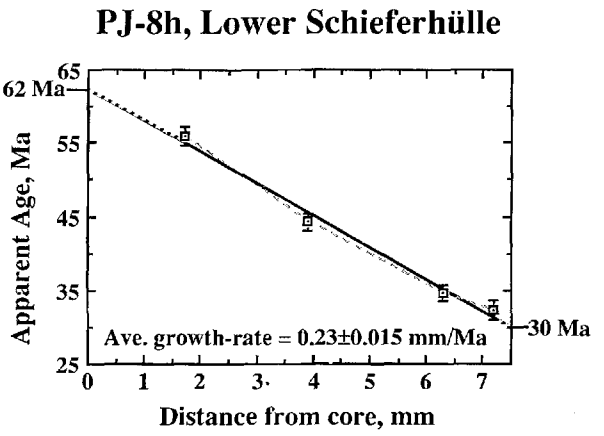

Fig. 10 Plot of the position of the centers of the PJ-8h garnet segments relative to the inferred core versus the age of each segment. The ages were calculated using the Rb-Sr composition of a matrix sample (Mx1) associated with the garnet

segments and the matrix $^{87}Rb/^{86}Sr$ (0.5%) and not the matrix $^{87}Sr/^{86}Sr$ (Christensen et al. 1989). This uncertainty is about $\pm$ 0.7 million years for the LSH garnet and $\pm$ 0.2 million years for the USH garnets. The uncertainty stated for the segment ages depends on the uncertainties in the Rb-Sr isotopic compositions of both the matrix and the garnet.

An additional uncertainty, which is difficult to quantify, is that introduced by the choice of the matrix sample. Some indication of the magnitude of this uncertainty is given by the LSH whole rock evolution line in Fig. 8. Use of the whole rock line gives an age for the LSH garnet "core" that is 4 Ma older that the age obtained using the matrix (Mx) sample immediately surrounding the garnet. The difference in calculated age using the matrix sample versus the whole rock is progressively less for the succeeding segments. Using the whole rock increases the calculated time interval of growth of the LSH by 7% due to the 7% lower Rb/Sr of the whole rock sample. A simple mass balance between garnet and matrix using their observed Rb and Sr concentrations and the modal abundance of garnet (~25%) approximates the Rb and Sr concentrations of the whole rock. Since the higher Rb/Sr of the matrix may be due to partitioning of Sr into garnet, the matrix Rb/Sr may have increased by as much as 7% during the period of garnet growth. Thus the time interval of growth for the earliest portion of the garnet using matrix-garnet isochrons may be underestimated by 7%, with the effect lessened for later portions.

In the case of sample HF-9a, calculation of ages for garnets A and B is nearly independent of the choice of matrix sample (i.e., Mx 1 vs. Mx 2). Using Mx 1 with garnet B reduces the rim segment age by 0.8 Ma and the core by 1.2 Ma, whereas using Mx 2 with garnet A raises the rim segment age by 0.8 Ma and the core by 1.4 Ma. Thus, in contrast to time intervals of 4.3 Ma (A) and 4.1 Ma (B) calculated using matrix samples adjacent to the garnets, the segments would define intervals of 4.9 Ma (A) and 3.7 Ma (B).

Shear-strain rate during USH garnet growth

Garnets of the USH, including the sample analyzed, typically show snowball textures. A garnet from the analyzed USH sample shows rotation of ~2.3 radians during growth, indicating a shear component of strain (Rosenfeld 1970) of ~4.6 during growth. This shear strain coupled with the average growth time of 5.4 $\pm$ 1.7 million years for the two HF-9a garnets yields a shear-strain rate of $2.7^{+1.2}_{-0.7} \times 10^{-14}\ s^{-1}$. For a sample from the Central Alps, Vance and O'Nions (1992) obtained an essentially identical shear-strain rate of $1.3^{+1.4}_{-0.5} \times 10^{-14}\ s^{-1}$. The rate for the Upper Schieferhülle is also comparable to the shear-strain rate calculated for Acadian age deformation recorded by nappe-contemporaneous garnet in SE Vermont

($2.4^{+1.6}_{-0.7} \times 10^{-14}\ s^{-1}$; Christensen et al. 1989). Assuming that the matrix behaved as a Newtonian fluid, the strain rate is equal to the ratio of the applied shear stress to the viscosity (Ranalli 1987, p. 70; Rosenfeld 1970, p. 87). Since the USH sample and the Vermont sample are similar in both mineralogy and pressure-temperature conditions during the deformation recorded by the garnets, one may conclude that the bulk rock viscosity was of similar magnitude in both cases. If this is correct, then the similar values of the shear-strain rate calculated for the Oligocene USH Alpine deformation and the Devonian Appalachian deformation imply that the stresses involved in the two deformation events were comparable.

Timing of tectonometamorphic events in the Tauern Window

The age and duration of garnet growth in the LSH provides constraints on the timing of high pressure metamorphism in the Tauern Window. Selverstone et al. (1984) and Selverstone and Spear (1985) describe pseudomorphs after lawsonite in both the LSH and USH, although the garnet *P-T* paths begin outside the stability field of lawsonite. Thus both the LSH and USH were first metamorphosed under blueschist conditions and subsequently subjected to a greenschist to amphibolite facies metamorphic overprint. The initiation of garnet growth in the LSH at about 62 Ma constrains the high pressure blueschist metamorphism to before 62 Ma. This is consistent with previous estimates that the early Alpine high pressure metamorphism is Late Cretaceous or Paleocene in age (Hawkesworth 1976; Janoschek and Matura 1980; Cliff et al. 1985); it is inconsistent with the contention that the Tauern Window was not covered by Austroalpine nappes until the Eocene (Lammerer 1988, p. 148).

The age of the thermal maximum within the Tauern Window has been debated much in recent literature, and in any case likely varies with structural position. In the area of the study, Raith et al. (1978) presented amphibole K/Ar data that Selverstone (1985) interpreted as dating the thermal maximum at 40 ± 5 Ma in the LSH. However, Blanckenburg and Villa (1988) demonstrated the probable influence of inherited radiogenic Ar on these ages, and obtained corrected ages of 18–20 Ma for LSH hornblendes. Phengite-whole rock Rb-Sr ages of 17.6 ± 0.2 Ma and 20.3 ± 0.3 Ma were obtained by Blanckenburg et al. (1989) from the same area. Because the calculated maximum temperature of 520–550 °C (Selverstone et al. 1984; Selverstone and Munoz 1987) overlaps the inferred closure temperatures for Rb-Sr in phengite and Ar diffusion in hornblende, Blanckenburg et al. (1989, p. 8) argue that the thermal maximum was attained at around 20 Ma. Based on the same data, Selverstone (1988, pp. 98–99) argued that the thermal maximum in the LSH was likely latest Oligocene in age, with the phengite and hornblende ages closing shortly thereafter; she also stated that the USH could have experienced its maximum temperature as much as 5–10 million years earlier, owing to its shallower structural position. However, the *P - T* paths of garnet growth calculated by Selverstone et al. (1984) and Selverstone and Spear (1985) indicate that considerable decompression occurred in association with only minor heating just prior to the thermal maximum in both units, suggesting that both the LSH and USH in this region may have remained within 20–50° C of the thermal maximum for a considerable length of time.

The USH and LSH garnet growth histories determined here provide an additional constraint on the timing of the thermal maximum. Within the error limits, garnet growth ceased in the LSH and USH nearly simultaneously at 30 ± 2 Ma. Garnet growth may halt in a metamorphic rock due to the exhaustion of the components required for growth or by initiation of cooling below the temperature required for reaction. It seems unlikely that the garnet-forming reaction would run to completion at the same time in two samples of differing bulk composition. Cooling would provide a much more likely explanation. On this basis the thermal maximum in the western Tauern Window was at around 30 Ma. The age of cessation of garnet growth in the Central Alps has also been found to be about 30 Ma (Vance and O'Nions 1992). The ~20 Ma amphibole and phengite ages discussed by Blanckenburg et al. (1989) thus likely represent cooling ages frozen in at temperatures 20–30° C below the LSH maximum; the 10 million years difference between these ages and the garnet rim ages of this study emphasize the long time interval over which the LSH remained near T_{max} during unroofing.

Time calibration of P-T paths

The calculated garnet growth rates and growth durations can be used to determine semi-quantitative pressure-time and temperature-time paths for the USH and the LSH based on the *P-T-t* paths for LSH and USH garnets presented by Selverstone et al. (1984), Selverstone and Spear (1985), Selverstone (1985) and J. Selverstone (unpublished data). These studies used major element zoning in garnet as a monitor of changing *P* and *T*, and mineral thermobarometry to fix the paths in *P-T* space. The assumptions are: (1) maintenance of equilibrium between the rim of the growing garnet and the surrounding matrix; (2) a constant and characterizable reaction assemblage or known reaction history; (3) a characterizable low-variance mineral assemblage; (4) a sufficient knowledge of the necessary thermodynamic data.

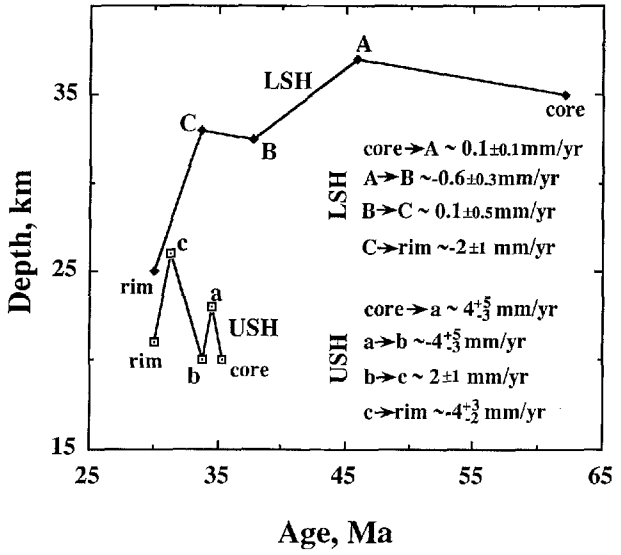

Fig. 11 Derived depth (pressure)-time paths for USH and LSH during garnet growth based on the *P-T* paths of Selverstone et al. (1984) and Selverstone and Spear (1985) and the measured garnet growth histories. Errors indicated for the approximate exhumation and burial rates reflect only the uncertainties in the geochronology

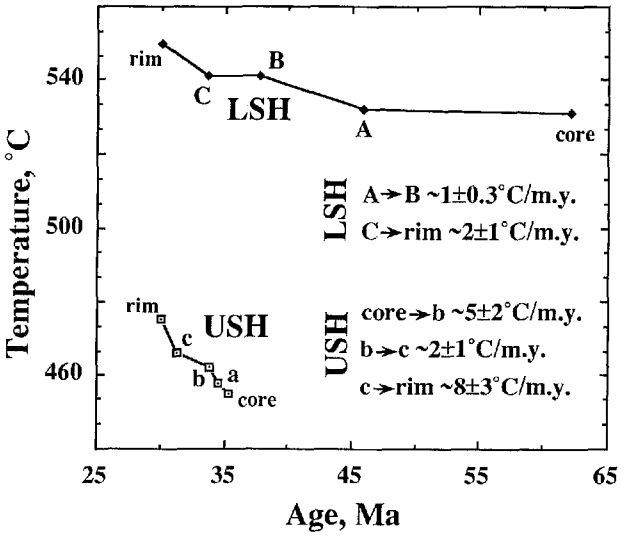

Fig. 12 Derived temperature-time paths for USH and LSH based on the *P-T* paths of Selverstone et al. (1984) and Selverstone and Spear (1985) and the measured garnet growth histories. Errors indicated for the approximate heating rates reflect only the uncertainties in the geochronology

Selverstone and Spear calculated a series of three pressure reversals in the *P-T-t* paths recorded by LSH and USH garnets during their growth. These reversals appear in every sample for which the calculations have been made, regardless of the mineral assemblage present (> 10 samples, 6 different assemblages; J. Selverstone, unpublished data). The ages of these reversals in the *P-T-t* paths of USH and LSH garnets are calculated here as though they occurred at the same relative positions within the garnets we analyzed as in those garnets used by Selverstone and Spear for their published *P-T-t* paths. Unfortunately, the garnets we analyzed occur in samples with mineral assemblages of too high variance to lend themselves to modeling of *P-T-t* paths from garnet zoning. However, the garnet zoning profiles are broadly similar to the LSH and USH profiles presented by Selverstone et al. (1984) and Selverstone and Spear (1985). The results of this section depend on the validity of the *P-T* paths derived from garnet zoning and the assumption that the *P-T* paths previously determined for LSH and USH garnets apply to the USH and LSH garnets we analyzed.

The derived depth-time (*P-t*) paths of the USH and LSH are displayed in Fig. 11. The calculated rate of depth change for the periods between reversals are also provided. The final increment of exhumation that is recorded by the USH and LSH garnets occurred at approximately the same time and at about the same rate within the errors, $\sim 4^{+3}_{-2}$ mm/year and $\sim 2 \pm 1$ mm/year respectively. The errors given reflect only the age uncertainties and do not include uncertainties in the barometry or in the correlation between our samples and those of Selverstone and Spear. The time interval, 4 ± 1 million years, between reversals B and C in the LSH path is nearly the same as the time interval, 2.5 ± 1 million years, between reversals b and c in the USH path. Selverstone (1985, 1988) has suggested that these *P* reversals in the *P-t* paths of the USH and LSH garnets correlate with one another. Between these reversals the *P-t* paths of the USH and LSH converge. Selverstone (1985, 1988) noted this decrease in the vertical separation of the LSH and USH and attributed it to ductile thinning of the USH. The average time, 3.2 million years, between the reversals B-b and C-c and the ~7 km decrease in the separation of the LSH and USH, indicates that this thinning occurred at a rate of ~2 km/million years. Prior to reversal C-c the USH and LSH appear to have followed different exhumation-burial histories. Alternatively the assumption that the garnets used to model the USH and LSH *P-T* paths grew over the same time intervals as the garnets analyzed here may not be valid.

The temperature-time paths of the USH and LSH garnets for the time they overlap appear to indicate a parallel thermal history (Fig. 12). Correlating the *P* and *T* of the LSH and USH paths suggests an increasing apparent thermal gradient with time, from about 6° C/km to about 20° C/km. This apparent increase in the thermal gradient is due to the decrease in separation between the USH and LSH. If real, then ductile thinning of the USH produced an increase in the thermal gradient by the compression of isotherms faster than thermal equilibration could occur. Again, the assumption that the garnets used to model the *P-T* path grew over the same time interval as the garnets analyzed here may not be valid.

The thermal maxima in the USH and LSH appear to have occurred at about 30 Ma (Fig. 12), although if the USH path is moved to the right to match the ages of reversal C-c the LSH may have reached its thermal maximum 1–3 million years later than the shallower USH. This would be generally consistent with numerical modeling of thrust-thickened crust with subsequent erosion (Thompson and England 1984), which predicts a time lag of the thermal maximum of about 0.5 to 1 million years per km of vertical separation. Thinning of the intervening section (Selverstone 1988) would likely reduce the magnitude of the time lag. Since the USH and LSH localities were probably separated vertically at this time by about 3–5 km (Selverstone 1988) a lag of up to a few million years between the thermal maxima in the LSH and the USH would be expected. However, such a lag is generally within the errors of the ages of cessation of USH and LSH garnet growth.

Summary and conclusions

Rb-Sr isotopic zonation was measured within single garnet crystals from samples of the Upper Schieferhülle (USH) and Lower Schieferhülle (LSH) from the western Tauern Window, Eastern Alps. Consistency of Sr isotopic zonation between two garnets in the USH sample indicates that the matrix Sr isotopic composition was homogeneous at a 2 cm scale. This zonation was used to calculate the rate and duration of garnet growth in the USH and LSH. The measured growth rates of the two USH garnets are $0.88^{+0.34}_{-0.19}$ mm/million years and $0.67^{+0.19}_{-0.13}$ mm/million years. The average duration of USH garnet growth was 5.4 ± 1.7 million years. The measured growth rate of the LSH garnet is 0.23 ± 0.015 mm/million years and the duration of growth is $\sim 32 \pm 2$ million years. The apparent ages of garnet segments were consistent between the two USH garnets and with the apparent age of garnet growth cessation observed in the LSH sample. This indicates that the apparent ages of garnet growth may provide useful constraints on ages of tectonometamorphic events.

The cessation of garnet growth was penecontemporaneous in the USH and LSH at 30 ± 2 Ma. This suggests that the thermal maximum in the USH and LSH was at around 30 Ma. Garnet growth in the LSH sample began as early as 62 ± 1.5 Ma. This constrains the high P/low T metamorphism in the Tauern Window to before that time.

Garnet growth in the USH between 35 and 30 Ma occurred during extensional shearing. The amount of shear deformation recorded by inclusion trails in garnet indicates an average shear-strain rate of $2.7^{+1.2}_{-0.7} \times 10^{-14}\ s^{-1}$, comparable to rates obtained from garnet in SE Vermont (Christensen et al. 1989) and in the Central Alps (Vance and O'Nions 1992).

Acknowledgements Financial support for the analyses reported in this paper was provided by NSF grants EAR 9118691 and EAR 8904696 to D. DePaolo/J. Rosenfeld. Field work to collect the samples was supported by NSF grants EAR 8606498 and EAR 8658145 to J. Selverstone. M. Reid provided helpful comments on an earlier version of the manuscript. The careful reviews of K. Mezger and R. Cliff are gratefully acknowledged.

References

Blanckenburg Fv, Villa IM (1988) Argon retentivity and argon excess in amphiboles from the garbenschists of the western Tauern Window, Eastern Alps. Contrib Mineral Petrol 100:1–10

Blanckenburg Fv, Villa IM, Baur H, Morteani G, Steiger RH (1989) Time calibration of a *PT*-path from the western Tauern Window, Eastern Alps: the problem of closure temperatures. Contrib Mineral Petrol 101:1 –11

Burton KW, O'Nions RK (1991) High-resolution garnet chronometry and the rates of metamorphic processes. Earth Planet Sci Lett 107:649–671

Christensen JN (1992) The Sr isotopic measurement of rates of tectonometamorphic processes: case studies in southwestern Vermont, USA and the Tauern Window, Eastern Alps. PhD diss, Univ Calif, Los Angeles

Christensen JN, Rosenfeld JL, DePaolo DJ (1988) Rates of tectonometamorphic processes: direct measuremcnt using Sr isotopic profiles of garnet porphyroblasts. EOS Trans Am Geophys Union 69:508

Christensen JN, Rosenfeld JL, DePaolo DJ (1989) Rates of tectonometamorphic processes from rubidium and strontium isotopes in garnet. Science 224:1465–1469

Cliff RA (1985) Isotopic dating in metamorphic belts. J Geol Soc London 142:97 110

Cliff RA, Droop GTR, Rex DC (1985) Alpine metamorphism in the south-east Tauern Window, Austria. 2. Rates of heating, cooling and uplift. J Mctamorphic Geol 3:403–415

Coghlan RAN (1990) Studies in diffusional transport: grain boundary transport of oxygen in feldspars, diffusion of oxygen, strontium and the REEs in garnet, and thermal histories of granitic intrusions in south-central Maine using oxygen isotopes. PhD diss, Brown Univ, Rhode Island

Hawkesworth CJ (1976) Rb/Sr geochronolgy of the Eastern Alps. Contrib Mineral Petrol 54:225–244

Hickmott DD, Shimizu N, Spear FS, Selverstone J (1987) Trace-element zoning in a metamorphic garnet. Geology 15:573–576

Huggins FE, Virgo D, Huckenholz HG (1977) Titanium-containing silicate garnets. II. The crystal chemistry of melanites and schorlomites. Am Mineral 62:646–665

Janoschek WR, Matura A (1980) Outline of the geology of Austria. Abh Geol Bundesant Austria 34:7–101

Lammcrer B (1988) Thrust-regime and transpression-regime tectonics in the Tauern Window (Eastern Alps). Geol Rundsch 77:143–156

Mezger K, Hanson GN, Bohlen SR (1989) U-Pb systematics of garnet: dating the growth of garnet in the late Archean Pikwitonei granulite domain at Cauchon and Natawahunan Lakes, Manitoba, Canada. Contrib Mineral Petrol 101:136–148

Mezger K, Bohlen SR, Hanson GN (1990) Metamorphic history of the Archean Pikwitonei granulite domain and Cross Lake subprovince, Superior Province, Manitoba, Canada. J Petrol 31:483–517

Mezger K, Essene EJ, Halliday AN (1992) Closure temperatures of the Sm-Nd system in metamorphic garnets. Earth Planet Sci Lett 113:397–409

Morteani G (1974) Petrology of the Tauern Window, Austrian Alps. Fortschr Mineral 52:195 220

Novak GA, Gibbs GV (1971) The crystal chemistry of the silicate garnets. Am Mineral 56:791 -825

Ranalli G (1987) Rheology of the Earth: deformation and flow processes in geophysics and geodynamics. Allen and Unwin, Boston

Raith M, Raase P, Kreuzer H, Müller P (1978) The age of the Alpidic metamorphism in the Western Tauern Window, Austrian Alps, according to radiometric dating. In: Cloos H, Roeder D, Schmidt K (eds) Alps, Apennines, Hellenides. Inter-Union Comm Geodynamics Sci Rep 38:140–148

Rosenfeld JL (1970) Rotated garnets in metamorphic rocks. Geol Soc Am Spec Pap 129

Schumacher JC (1991) Empirical ferric iron corrections: necessity, assumptions, and effects on selected geothermobarometers. Mineral Mag 55:3–18

Selverstone J (1985) Petrologic constraints on imbrication, metamorphism, and uplift in the SW Tauern Window, Eastern Alps. Tectonics 4:687–704

Selverstone J (1988) Evidence for east-west crustal extension in the Eastern Alps: implications for the unroofing history of the Tauern Window. Tectonics 7:87–105

Selverstone J, Munoz JL (1987) Fluid heterogeneities and hornblende stability in interlayered graphitic and nongraphitic schists (Tauern Window, Eastern Alps). Contrib Mineral Petrol 96:426–440

Selverstone J, Spear FS (1985) Metamorphic *P-T* paths from pelitic schists and greenstones from the south-west Tauern Window, Eastern Alps. J Metamorphic Geol 3:439–465

Selverstone J, Spear FS, Franz G, Morteani G (1984) High-pressure metamorphism in the SW Tauern Window, Austria: *P-T* paths from hornblende-kyanite-staurolite schists. J Petrol 25:501–531

Selverstone J, Morteani G, Staude J-M (1991) Fluid channeling during ductile shearing: transformation of granodiorite into aluminous schist in the Tauern Window, Eastern Alps. J Metamorphic Geol 3:439–465

Shannon RD (1976) Revised effective ionic radii and systematic studies of interatomic distances in halides and chalcogenides. Acta Crystallogr A 32:751–767

Thompson AB, England PC (1984) Pressure-temperature-time paths of regional metamorphism. II. Their inference and interpretation using mineral assemblages in metamorphic rocks. J Petrol 25:929–955

Vance D, O'Nions RK (1990) Isotopic chronometry of zoned garnets growth kinetics and metamorphic histories. Earth Planet Sci Lett 97:227–240

Vance D, O'Nions RK (1992) Prograde and retrograde thermal histories from the central Swiss Alps. Earth Planet Sci Lett 114:113–129

Zeitler PK (1989) The geochronolgy of metamorphic processes. In: Daly JS, Cliff RA, Yardley BWD (eds) Evolution of metamorphic belts. Geol Soc London Spec Publ 43:131–147